# Reduced-Order Model-Based Feedback Control of Flow Over an Obstacle Using Center Manifold Methods

**Coşku Kasnakoğlu**[1]
Department of Electrical and Electronics Engineering,
TOBB University of Economics and Technology,
Ankara 06560, Turkey
e-mail: kasnakoglu@etu.edu.tr

**R. Chris Camphouse**
Carlsbad Programs Group,
Performance Assessment and Decision Analysis Department,
Sandia National Laboratories,
Carlsbad, NM 88220

**Andrea Serrani**
Department of Electrical and Computer Engineering,
The Ohio State University,
Columbus, OH 43210

*In this paper, we consider a boundary control problem governed by the two-dimensional Burgers' equation for a configuration describing convective flow over an obstacle. Flows over obstacles are important as they arise in many practical applications. Burgers' equations are also significant as they represent a simpler form of the more general Navier–Stokes momentum equation describing fluid flow. The aim of the work is to develop a reduced-order boundary control-oriented model for the system with subsequent nonlinear control law design. The control objective is to drive the full order system to a desired 2D profile. Reduced-order modeling involves the application of an $\mathcal{L}_2$ optimization based actuation mode expansion technique for input separation, demonstrating how one can obtain a reduced-order Galerkin model in which the control inputs appear as explicit terms. Controller design is based on averaging and center manifold techniques and is validated with full order numerical simulation. Closed-loop results are compared to a standard linear quadratic regulator design based on a linearization of the reduced-order model. The averaging/center manifold based controller design provides smoother response with less control effort and smaller tracking error.* [DOI: 10.1115/1.3023122]

## 1 Introduction

Boundary flow control has received significant research attention during the last decades. Most flow applications modeled by Burgers' and Navier–Stokes (NS) equations require that actuation and sensing be limited to the boundary. Correspondingly, boundary control studies on these equations are of particular interest. Examples of recent progress in this area include Smaoui [1] who analyzed the dynamics of the forced Burgers' equation subject to both Neumann boundary conditions and periodic boundary conditions using boundary and distributed controls. Hinze and Kunisch [2] devised second-order methods for open loop optimal boundary control problems governed by the nonstationary Navier–Stokes system. Nonlinear boundary control of coupled Burgers' equations was studied by Kobayashi and Oya [3]. Park and Lee [4] studied boundary control of the Navier–Stokes equation by empirical reduction of modes. Global stabilization of Burgers' equation by boundary control was studied by Kristic [5], where nonlinear boundary control laws were derived that achieve global asymptotic stability of both the viscous and the inviscid Burgers' equation, using both Neumann and Dirichlet boundary control. Aamo et al. [6] achieved enhancement of mixing by implementing boundary control for Navier–Stokes equations describing 2D channel flow.

The modeling aspect of the boundary flow control problem has traditionally focused on very accurate and complex high-order models, e.g., discretized flow models with millions of state variables [7]. For systematic control system design, however, models of such large dimension are computationally intractable. A means of obtaining reduced-order control-oriented models is necessary. Recent research efforts have pursued the development of reduced models amenable to boundary flow control. A variety of approaches have been undertaken, including those based on flow physics and empirical identifications from experiment. One of the many examples of the latter includes Kook et al. [8], who determined open-loop transfer functions for low-speed flows at several different flow velocities by observing the response to forcing. As to the modeling approaches using fluid physics, Rowley et al. [9] Noack et al. [10] and Rempfer [11] could be listed as a few examples whom all investigated a common methodology: One first starts from the infinite dimensional NS equations describing the evolution of fluid flows. Temporal snapshots of flow behavior are generated via simulation or experiment. An energy-optimal set of basis vectors are constructed from the snapshot ensemble via proper orthogonal decomposition (POD). The NS equations are projected onto the space spanned by the POD basis. This procedure is called the Galerkin projection (GP) and yields a finite dimensional system of differential equations that approximate the original system dynamics in the energy optimal sense. A reduced-order system model obtained in this fashion is called a *Galerkin model* (GM) and the methodologies used to obtain such model from the original NS equations is termed *model reduction*. A detailed description of the POD-GP method can be found in Holmes et al. [12]. Galerkin models obtained as such have been used extensively to develop controls for flow applications, including feedback control of cylinder wakes [10,13,14], control of cavity flows [9,15–17], and optimal control of vortex shedding [18].

A major difficulty with many reduced-order modeling approaches, including the POD-GP procedure above, is that the boundary conditions get absorbed in the model coefficients, and do not appear explicitly. For this reason, one must find a way to incorporate the effects of the input into the dynamics. For instance, Hogberg et al. [19] studied convolution kernels to incorporate the effect of the forcing input for feedback control and estimation of linearized Navier–Stokes systems. Camphouse [20,21] used weakly formed Galerkin projections in combination with proper orthogonal decomposition to obtain reduced-order state-space models with explicit boundary control input and applied the technique to a nonlinear convection feedback control

[1]Corresponding author. This material is declared a work of the U.S. Government and is not subject to copyright protection in the United States. Approved for public release; distribution is unlimited.

Contributed by the Dynamic Systems, Measurement, and Control Division of ASME for publication in the JOURNAL OF DYNAMIC SYSTEMS, MEASUREMENT, AND CONTROL. Manuscript received December 8, 2007; final manuscript received September 8, 2008; published online December 8, 2008. Assoc. Editor Fen Wu.

problem. For Burgers' equations, an approach based on partitioning the flow domain into subdomains to make the free boundary condition appear as a control input in the reduced-order models was investigated by Efe and Ozbay [22]. Kasnakouglu et al. [23] augmented the POD expansion with actuation modes selected by solving a particular $\mathcal{L}_2$ optimization problem, resulting in reduced-order models where the input appears as an explicit term.

Effective control of the flow over an obstacle has relevance to many applications in government and industry. Early works by Hunt et al. [24] studied flows around free or surface-mounted obstacles using kinematical theory. More recent studies such as those done by Orellano and Wengle [25] utilize direct numerical simulation (DNS) and large eddy simulation (LES) of manipulated turbulent boundary layer flow over a surface-mounted fence. Modeling and control of vortex shedding and cylinder wakes for bluff body applications also belong to this category [10,13,14,18]. In this paper, we consider a case study of a boundary flow control model problem describing convective flow over an obstacle. The governing equation for the model is the two-dimensional Burgers' equation. The case study on the sample problem in this paper will address both reduced-order modeling and nonlinear control design, with the control objective of driving the system state to a desired 2D profile. The reduced-order modeling involves the application of an $\mathcal{L}_2$ optimization-based actuation mode expansion for input separation developed in our earlier works [23], demonstrating how one can obtain a reduced-order Galerkin model in which the control inputs appear as explicit terms. Once the reduced-order model is available, two different control design methods are employed to achieve the desired objective: (1) A design based on averaging and center manifold (CM) techniques [26,27], and (2) a linear quadratic regulator (LQR) design based on a linearization of the reduced-order model [21]. While controllers resulting from both methods will have the same linear structure, the averaging/center manifold method is a technique that goes beyond Jacobian linearization as far as the domain of validity is concerned. The averaging/center manifold approach is used to obtain a simplified nonlinear model with a structure that can be exploited for control design. Looking at the reduced dynamics on the center manifold allows one to cast the control design as a parameter optimization problem on a nonlinear system with reduced dimension. It will be seen through full order simulations that, while both controllers achieve the desired objective, the averaging/center manifold based controller design results in a smoother response, less control effort, and smaller tracking error over the problem domain.

## 2 Problem Description

The case study considered in this paper is a distributed parameter system, which models convective flow over a rectangular obstacle [21,28]. The choice of a rectangle for the obstacle is actually arbitrary and without loss of generality, as at no point in this paper we shall utilize a procedure that is dependent on this shape. A reduced-order model of this system will be developed for feedback control design. Let $\Omega_1 \subseteq \mathbb{R}^2$ be the rectangle given by $(a,b]\times(c,d)$. Let $\Omega_2 \subseteq \Omega_1$ be the rectangular domain given by $[a_1,a_2]\times[b_1,b_2]$ where $a<a_1<a_2<b$ and $c<b_1<b_2<d$. The problem domain $\Omega$ is given by $\Omega=\Omega_1\backslash\Omega_2$, where $\Omega_2$ is the obstacle. Dirichlet boundary controls are located on the obstacle bottom and top, denoted by $\Gamma_{\text{bottom}}$ and $\Gamma_{\text{top}}$, respectively. A schematic of the problem geometry is given in Fig. 1. The dynamics of the system are described by the two-dimensional Burgers' equation.

$$\frac{\partial}{\partial t}q(x,y,t) + \nabla \cdot F(q) = \frac{1}{\text{Re}}\Delta q(x,y,t) \tag{1}$$

where $t>0$ is the temporal variable, and $(x,y)$ are the coordinates of a point in $\Omega$. In Eq. (1), $F(q)$ has the form

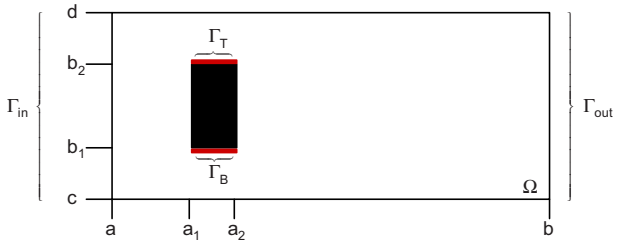


**Fig. 1 Geometry of the problem**

$$F(q) = \begin{bmatrix} k_1\dfrac{q^2(x,y,t)}{2} & k_2\dfrac{q^2(x,y,t)}{2} \end{bmatrix}^T \tag{2}$$

where $k_1$ and $k_2$ are non-negative constants. This equation has a convective nonlinearity like the one found in the Navier–Stokes momentum equation modeling fluid flow [29]. The quantity Re, a non-negative constant, is analogous to the Reynolds number in the Navier–Stokes momentum equation. We will also write Eq. (1) in compact form as

$$\dot{q} = X(q) \tag{3}$$

where $X(q)=-\nabla\cdot F(q)+\text{Re}^{-1}\Delta q$. For simplicity, boundary controls are assumed to be separable. With this assumption, we specify conditions on the obstacle bottom and top of the form, as follows:

$$q(x,y,t) = \gamma_{\text{bottom}}(t)\Psi_B(x) \quad \text{for} \quad (x,y) \in \Gamma_{\text{bottom}} \tag{4}$$

$$q(x,y,t) = \gamma_{\text{top}}(t)\Psi_T(x) \quad \text{for} \quad (x,y) \in \Gamma_{\text{top}} \tag{5}$$

where $\gamma_{\text{bottom}}(t)$ and $\gamma_{\text{top}}(t)$ are the control inputs on the bottom and top of the obstacle, respectively. The profile functions $\Psi_B(x)$ and $\Psi_T(x)$ describe the spatial influence of the controls on the boundary. A parabolic inflow condition is specified as follows:

$$q(x,y,t) = f(y) \quad \text{for} \quad (x,y) \in \Gamma_{\text{in}} \tag{6}$$

At the outflow, a Neumann condition is specified according to the following relationship:

$$\frac{\partial}{\partial x}q(x,y,t) = 0 \quad \text{for} \quad (x,y) \in \Gamma_{\text{out}} \tag{7}$$

For notational convenience, the remaining boundary is denoted by $\Gamma_U$. We require that values of $q$ be fixed at zero along $\Gamma_U$ as time evolves. The resulting boundary condition is of the form

$$q(x,y,t) = 0 \quad \text{for} \quad (x,y) \in \Gamma_U \tag{8}$$

The initial condition of the system is given as

$$q(0,x,y) = q_{\text{init}}(x,y) \in \mathcal{L}_2(\Omega) \tag{9}$$

## 3 Reduced-Order Modeling

In this paper, the system described in Sec. 2 will serve as a surrogate to develop control techniques amenable to flow systems. The first step that we will take toward this goal is model reduction, which can be justified as follows: For almost any flow control configuration, there are two fundamental obstacles that lead one to reduce the size of the system beforehand. The first is that the governing equations for flow systems are infinite dimensional distributed parameter systems such as Navier–Stokes or Burgers' equations. While in theory it is possible to develop a theoretical controller for that distributed parameter system and then discretize the control, this problem is, in general, extremely difficult, if not impossible, for such complicated partial differential equations (PDEs). An alternative approach would be to discretize the system and then develop a "full-order" controller from the discretized system, followed by an order reduction of the full order controller. This approach is also very difficult if not impossible to realize for most fluid systems, as a typical discretized flow model describes

thousand to millions of state variables. For a system this large, calculating a full order controller from the full order discretized model will almost always be computationally intractable. These two obstacles together force one to reduce the system order prior to developing the control law. As we are using the model problem as a surrogate for "real" flow systems, we are limiting ourselves to approaches that would actually lend themselves to those kinds of systems. While developing a full order controller is clearly not one of these approaches, developing a controller based on a reduced order model would definitely qualify, and hence, it is direction that will be investigated in this paper.

In this section, we will first provide a brief summary of the classical POD/GP approach to reduced-order modeling of flow systems, and then apply an $\mathcal{L}_2$ optimization method for input separation, as proposed in Ref. [23].

**3.1 Classical POD/GP Based Modeling.** Let $\mathbb{H}$ be a real Hilbert space with inner product $\langle\cdot,\cdot\rangle:\mathbb{H}\times\mathbb{H}\to\mathbb{R}$. Throughout the paper, we will focus our attention to $\mathbb{H}=\mathcal{L}_2(\Omega,\mathbb{R})$ with the standard inner product $\langle h_1,h_2\rangle=\int\int_{(x,y)\in\Omega}h_1(x,y)h_2(x,y)dxdy$ for $h_1,h_2\in\mathcal{L}_2$, although the results apply to other Hilbert spaces as well. Let $q:\Omega\times\mathbb{R}_+\to\mathbb{R}$, $q(\cdot,\cdot,t)\in\mathbb{H}$, $q(x,y,\cdot)\in\mathcal{C}^k$ and $k\in\mathbb{N}$. Let $q_k(x,y)=q(x,y,t_k)$ be a *snapshot* taken at time $t_k$ and let $\{q_k\}_{k=1}^M\subset\mathbb{H}$ be an ensemble of $M\in\mathbb{N}$ snapshots collected at times $\{t_k\}_{k=1}^M$. Let $q_0:=E[q_j]$ where $E$ is a linear averaging operation $E[q_j]=M^{-1}\Sigma_{i=1}^M w_j q_j$ for given weights $w_j>0$. From the snapshots $\{q_k\}_1^M$, the POD procedure is used to obtain a set of *POD modes* $\{\varphi_i\}_1^N\subset\mathbb{H}$ and a set of *modal coefficients* $\{a_i\}_1^N\subset\mathbb{R}$ so that[2]

$$q(x,y,t)\approx q_0+\sum_{i=1}^{N}a_i(t)\phi_i(x,y) \tag{10}$$

A dynamical system that approximates the flow dynamics can be obtained by Galerkin projection as $\dot{r}=X_S(r)$, where $r:=q_0+a_j\varphi_j\in S$, and $S:=q_0+\text{span}\{\varphi_1,\ldots,\varphi_N\}$. Simplification yields the following set of nonlinear ordinary differential equations (ODEs):

$$\dot{a}_k=\langle X(r),\phi_k\rangle,\quad k=1,\ldots,N \tag{11}$$

Details of the modeling process summarized above can be found in Refs. [9,12]. Note that, at this stage, the effect of actuation is still embedded in the coefficients of the Galerkin system and does not appear explicitly in Eq. (11). We will remedy this situation in Sec. 3.2.

**3.2 Input Separation Through $\mathcal{L}_2$ Optimization.** The input separation method applied in this work relies on an expansion of the flow field in terms of *baseline* POD modes and *actuation modes*. The baseline modes $\varphi_i$ are extracted from the unactuated flow using a standard POD procedure as described in Sec. 3.1. As will be explained in more details in Sec. 3.3, since the inlet will be treated as a pseudoinput for modeling purposes, the unactuated flow means that the flow value at the top and bottom of the obstacle, as well as that at the inlet is set to zero. An *innovation* flow field is defined as $\tilde{q}(x,y,t):=q(x,y,t)-P_Sq(x,y,t)$, where $S:=q_0+\text{span}\{\varphi_i\}$ and $P_S$ is the projection operator onto $S$. Forced flow snapshots are projected onto the span of the baseline POD modes to obtain the portion of the controlled flow that is recovered by $S$, whereas the innovation yields the information, which is not captured by $S$ and is due to the effect of the actuation. Next, the actuation modes are built from the innovations using the approach described below.

For simplicity, let us first assume that we only use a single scalar input $\gamma$. For our sample problem, this corresponds to using only one of the inputs available, say, $\gamma_{\text{top}}$. We then consider an expansion of the form

$$q\approx q_0+\sum_{i=1}^{N}a_i\phi_i+\gamma\psi \tag{12}$$

where the actuation mode $\psi$ is to be chosen so as to minimize the energy not captured by such an expansion. An optimization problem on the Hilbert space $\mathbb{H}$ can be defined as finding $\psi^*=\arg\min_{\psi\in\mathbb{H}}J(\psi)$, where $J(\psi):=E[\|\tilde{q}_k-\gamma_k\psi\|^2]$. The element $\psi^*\in\mathbb{H}$ will be chosen as the actuation mode. The squared norm of the velocity represents the energy contained in the flow. Therefore, among all augmented POD expansions in the form given in Eq. (12) where *the input $\gamma$ directly appears as the coefficient of $\psi$*, the choice $\psi=\psi^*$ is optimal, in the sense that the energy not captured by this expansion achieves its minimum for $\psi=\psi^*$. The theorem below summarizes the main result.

Theorem 3.1

1. The minimum value of the function $J$ is achieved at $\psi^*=E[\gamma_k\tilde{q}_k]/E[(\gamma_k)^2]$.
2. $\psi^*\in\mathbb{H}$.
3. $\psi^*\perp\varphi_i$ for $i=1,\ldots,N$.

*Proof.* See the Appendix.

The Galerkin model obtained by substituting Eq. (12) into Eq. (11) has the form

$$\dot{a}_i=C_i+L_{ik}a_k+L_{\text{in},i}\gamma+Q_{ijk}a_ka_j+Q_{\text{ain},ik}a_k\gamma+Q_{\text{in},i}\gamma^2$$

The procedure outlined extends easily for systems with additional inputs. Starting with the simplest case where only two inputs $\gamma_1$ and $\gamma_2$ are available, given an ensemble of actuated flows $\{q_k\}_1^M\subset\mathbb{H}$ and an ensemble of actuation values $\{\gamma_{1k}\}_1^M\subset\mathbb{R}$ and $\{\gamma_{2k}\}_1^M\subset\mathbb{R}$, one obtains the actuation mode $\psi_1$ for the input $\gamma_1$ using the same procedure described above, that is,

$$\psi_1=\arg\min_{\psi\in H}E(\|\tilde{q}_k-\gamma_{1k}\psi\|)$$

Now let us define

$$\breve{q}_k:=q_k-P_{S_1}q_k$$

where $S_1:=\text{span}\{\varphi_1,\ldots,\varphi_N,\psi_1\}$. One can now use the same procedure described above with $\breve{q}$ replacing $q$ to obtain an actuation mode for $\gamma_2$ as

$$\psi_2=\arg\min_{\psi\in H}E(\|\breve{q}_k-\gamma_{2k}\psi\|)$$

with $\psi_2\perp S_1$. This yields an actuated POD expansion of the form

$$q=q_0+\sum_{i=1}^{N}a_i\phi_i+\gamma_1\psi_1+\gamma_2\psi_2$$

It is possible to extend the procedure as many times as needed if there are additional inputs. If one has, say $N_{\text{in}}$ inputs, then it is possible to obtain an expansion of the form

$$q=q_0+\sum_{i=1}^{N}a_i\phi_i+\sum_{i=1}^{N_{\text{in}}}\gamma_i\psi_i$$

The Galerkin system corresponding to the above expansion will be of the form

$$\dot{a}_i=C_i+L_{ik}a_k+L_{\text{in},ik}\gamma_k+Q_{ijk}a_ka_j+Q_{\text{ain},ijk}a_k\gamma_j+Q_{\text{in},ijk}\gamma_k\gamma_j \tag{13}$$

which can be expressed in compact form as

$$\dot{a}=C+La+L_{\text{in}}\gamma+Q(a,a)+Q_{\text{ain}}(a,\gamma)+Q_{\text{in}}(\gamma,\gamma) \tag{14}$$

where $C$ is constant, $L$ and $L_{\text{in}}$ are linear, and $Q$, $Q_{\text{in}}$, and $Q_{\text{ain}}$ are quadratic in their arguments. The initial condition $a_0$ for the reduced order model is obtained as

[2]Whenever convenient, we will use Einstein notation to omit summation signs and write $q(xy,t)\approx q_0+a_i(t)\varphi_i(x,y)$ in place of Eq. (10).

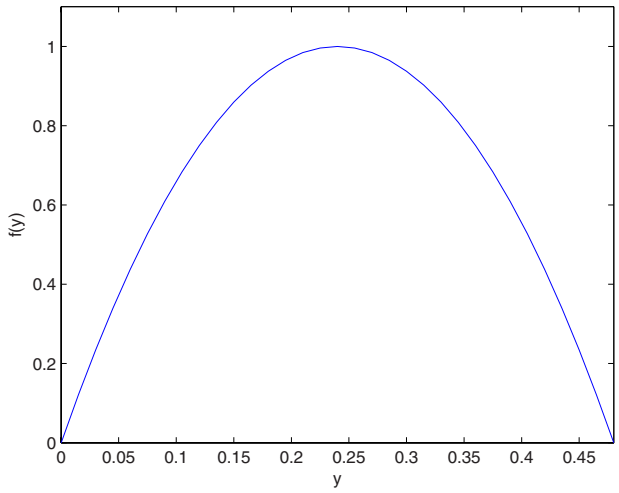


**Fig. 2 Inlet condition on the left boundary of the domain**

$$a_0 = P_S q_{\text{init}}$$

**3.3 Application to the Model Problem.** The methodology presented in Sec. 3.2 is used to obtain a reduced-order model for the problem described in Sec. 2. In addition to analytical derivations, we will also provide numerical simulation results in parallel. Throughout this paper, for numerical simulations a positive parabolic profile with unit maximum amplitude is specified for the inlet condition in boundary condition (6), as shown in Fig. 2. In Eq. (2), we set $k_1=1$ and $k_2=0$ in order to obtain solutions that convect from left to right for the positive inlet. In addition, we set Re=300. Parameters for the problem domain $\Omega$ are specified as $a=0$, $b=0.99$, $c=0$, $d=0.48$, $a_1=0.15$, $a_2=0.24$, $b_1=0.15$, $b_2=0.33$, and the problem domain is discretized, resulting in a uniform grid with spatial step-size $h=0.015$. We utilize the finite difference scheme in Refs. [21,28] to solve the model problem numerically with a semidiscrete Runge–Kutta algorithm.

The first step of the modeling process is to build a baseline model from baseline snapshots. We will define the baseline conditions as the those where the control inputs as well as the inlet flow vanish. Note that the inlet flow is not an actual control input. However, to improve accuracy of the reduced-model, we regard it as a pseudoinput, denoted by $\gamma_{\text{inlet}}$. The inlet flow is present for $\gamma_{\text{inlet}}=1$ and vanishes for $\gamma_{\text{inlet}}=0$. Figure 3 shows the snapshots of the solution of the system (1) under no forcing and no inlet. The initial condition is shown in the upper left plot. The lower right plot is of the steady state solution. Figure 4 is a plot of baseline modes constructed from the baseline snapshot ensemble. The number of baseline modes taken is four, corresponding to $N=4$ in the baseline POD expansion. This value is a good compromise between the amount of energy captured (99.8564%) and the complexity of the reduced-order model. Higher values of $N$ result in higher-order models that capture more energy, but these models are less tractable from a control design perspective. In addition to the baseline modes, actuation modes are obtained using actuated snapshots of the system. Figures 5–7 show the system under actuation at the inlet, at the inlet and top of the obstacle, and at the inlet and bottom of the obstacle, respectively. When present, the actuation signal applied from the top or bottom of the obstacle is shown in Fig. 8. Snapshots from these flow conditions are used to build the actuation modes $\psi_{\text{inlet}}$, $\psi_{\text{top}}$, and $\psi_{\text{bottom}}$, which are shown in Fig. 9. Following the procedure outlined in Sec. 3, one obtains the Galerkin system for Eq. (1) having the form in Eq. (13) where $\gamma=[\gamma_{\text{top}}\gamma_{\text{bottom}}\gamma_{\text{inlet}}]^T$ and

$$C_i := \left\langle -k_1 q_0 \frac{\partial}{\partial x} q_0 - k_2 q_0 \frac{\partial}{\partial y} q_0 + \mu\left(\frac{\partial^2}{\partial x^2} q_0 + \frac{\partial^2}{\partial y^2} q_0\right), \phi_i \right\rangle$$

$$Q_{\text{ain},ijk} := \left\langle -k_1 \phi_j \frac{\partial}{\partial x} \psi_k - k_2 \phi_j \frac{\partial}{\partial y} \psi_k - k_1 \psi_j \frac{\partial}{\partial x} \phi_k - k_2 \psi_j \frac{\partial}{\partial y} \phi_k, \phi_i \right\rangle$$

$$Q_{\text{in},ijk} := \left\langle -k_1 \psi_j \frac{\partial}{\partial x} \psi_k - k_2 \psi_j \frac{\partial}{\partial y} \psi_k, \phi_i \right\rangle$$

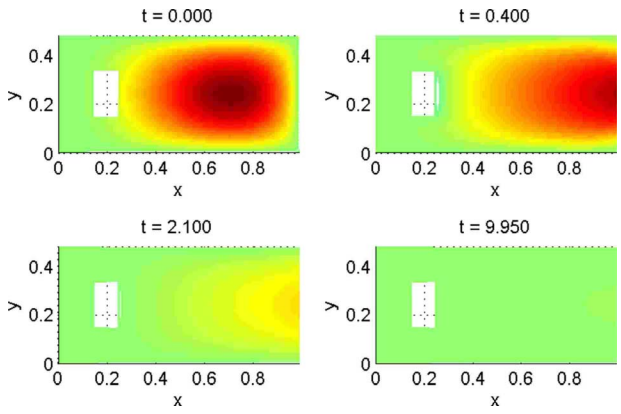


**Fig. 3 Flow with no inlet and no excitation**

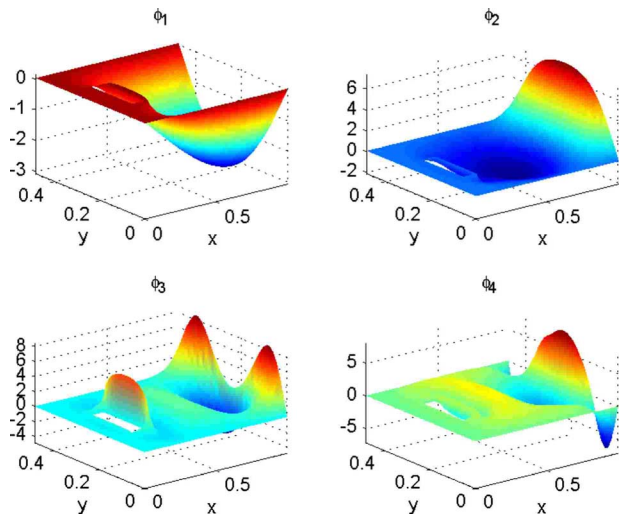


**Fig. 4 Baseline POD modes**

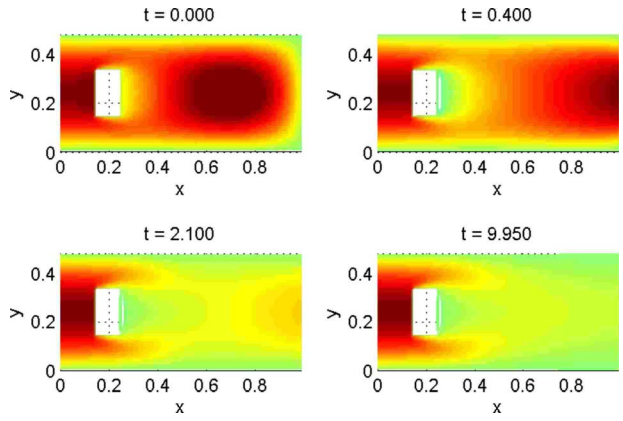


**Fig. 5 Flow with excitation at the inlet**

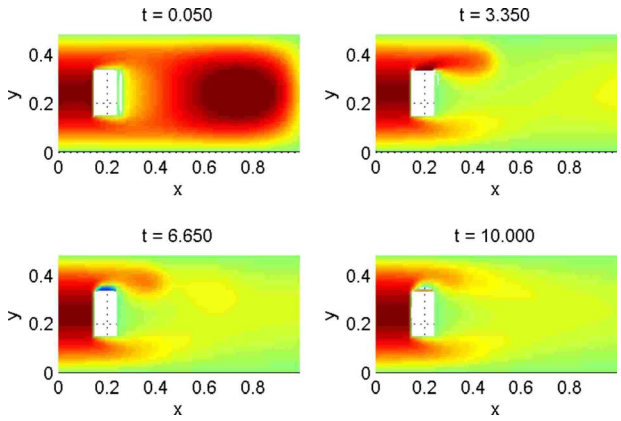


**Fig. 6 Flow with excitation at the inlet and at the top**

$$L_{\text{in},ik} := \left\langle -k_1 q_0 \frac{\partial}{\partial x}\psi_k - k_2 q_0 \frac{\partial}{\partial y}\psi_k - k_1 \psi_k \frac{\partial}{\partial x} q_0 - k_2 \psi_k \frac{\partial}{\partial y} q_0 + \mu\left(\frac{\partial^2}{\partial y^2}\psi_k + \frac{\partial^2}{\partial x^2}\psi_k\right), \phi_i \right\rangle$$

$$Q_{ijk} := \left\langle -k_1 \phi_j \frac{\partial}{\partial x}\phi_k - k_2 \phi_j \frac{\partial}{\partial y}\phi_k, \phi_i \right\rangle$$

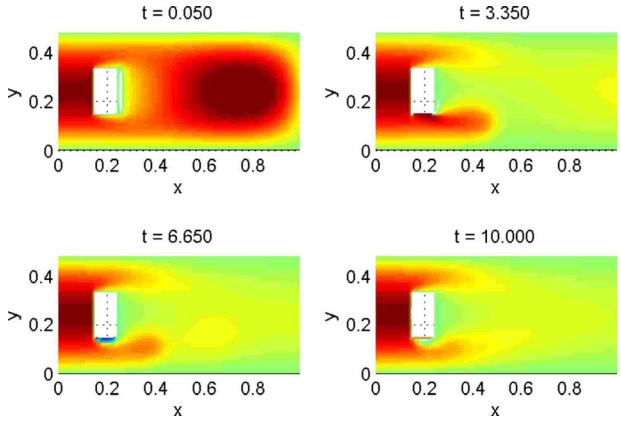


**Fig. 7 Flow with excitation at the inlet and at the bottom**

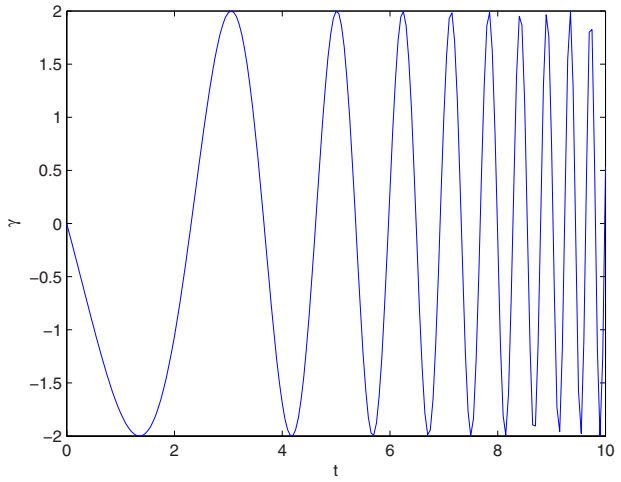


**Fig. 8 Excitation signal for system identification**

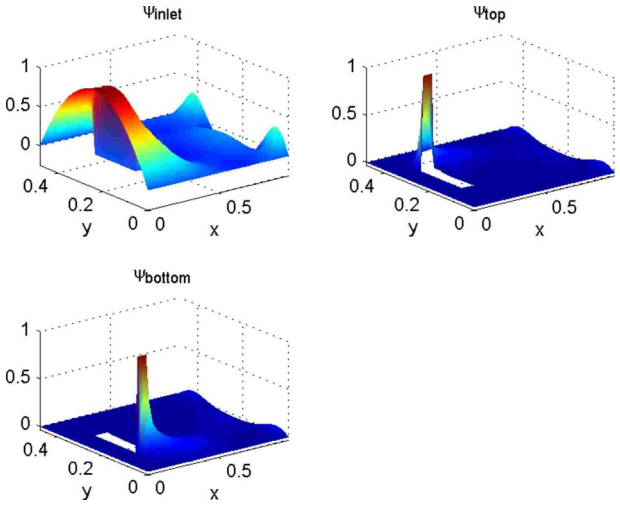


**Fig. 9 Actuation modes**

$$L_{ik} := \left\langle -k_1 \phi_k \frac{\partial}{\partial x} q_0 - k_2 \phi_k \frac{\partial}{\partial y} q_0 + \mu\left(\frac{\partial^2}{\partial y^2}\phi_k + \frac{\partial^2}{\partial x^2}\phi_k\right) - k_1 q_0 \frac{\partial}{\partial x}\phi_k - k_2 q_0 \frac{\partial}{\partial y}\phi_k, \phi_i \right\rangle$$

As a test of the ability of the Galerkin model to represent the full order system, consider the excitation shown in Fig. 10 applied from the top and bottom of the obstacle. The results from this excitation are shown in Fig. 11. In Fig. 12, the response of the Galerkin system is compared to modal coefficient values obtained by projecting actuated snapshots onto the reduced basis. Figure 13 shows the flow reconstructed as $q = q_0 + a_i \varphi_i + \gamma_{\text{inlet}} \psi_{\text{inlet}} + \gamma_{\text{top}} \psi_{\text{top}} + \gamma_{\text{bottom}} \psi_{\text{bottom}}$ using the the modal coefficients $a_i$ obtained the reduced-order model. By examining these figures, one sees that the reduced-order Galerkin model response captures the qualitative behavior of the projected values with good quantitative agreement. As discussed above, increasing $N$ results in a high-order model with better quantitative performance. However, this would make the control design more involved and is therefore undesirable. We emphasize here that the aim of this work is to develop a reduced-order system model suitable for nonlinear control design methods. Good control design results in controllers robust enough

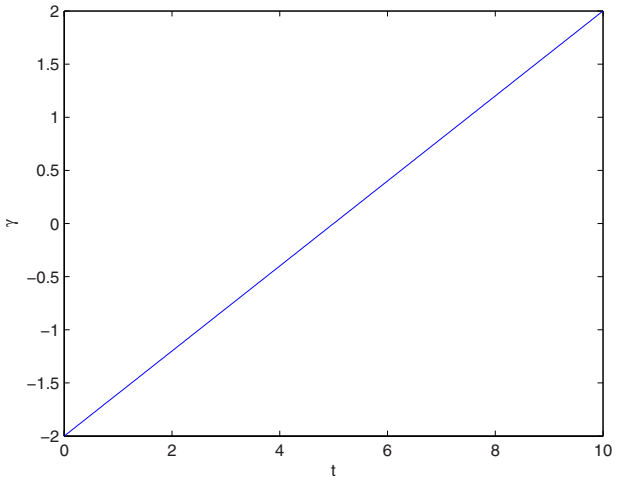


**Fig. 10 Excitation signal for model validation**

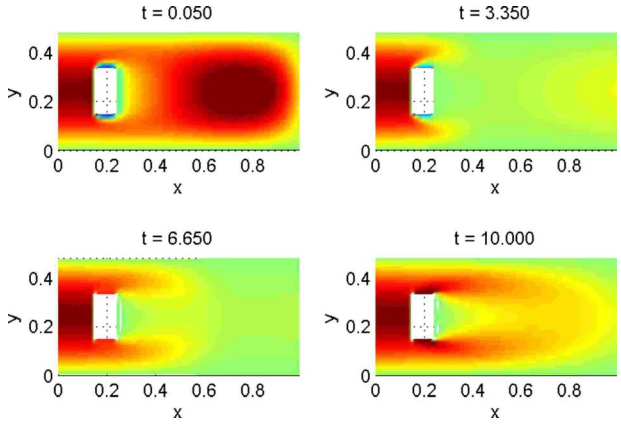


**Fig. 11 Flow with test excitation signal applied to top and bottom**

to compensate for reasonable inaccuracies in the reduced model. As a result, we deem the accuracy illustrated in Fig. 12 to be satisfactory for our objectives.

## 4 Control Design

In this section, a control law will be designed on the basis of the reduced-order model derived in Sec. 3.3. We will employ two different approaches: (1) A design based on averaging and center manifold techniques [26,27] and (2) LQR design based on the linearization of the model [21]. For the control objective, we specify a fixed 2D reference profile $q_d$ and design a controller to drive the trajectories of the systems to this profile. The profile reference is chosen to be a nonequilibrium state of the system in absence of an appropriate control action. Projecting $q_d$ onto the baseline POD basis yields the reference modal coefficients $a_d = (a_{d_i})_{i=1}^N$ for the reduced-order model, that is,

$$a_d = P_S q_d$$

As the reference is selected so that there exists a $\gamma_d$ such that

$$C + La_d + L_{\text{in}}\gamma_d + Q(a_d, a_d) + Q_{\text{in}}(\gamma_d, \gamma_d) + Q_{\text{ain}}(a_d, \gamma_d) = 0 \tag{15}$$

one can define a shift of coordinates $\tilde{a} = a - a_d$, $\tilde{\gamma} = \gamma - \gamma_d$, which yields

$$\dot{\tilde{a}} = \tilde{L}\tilde{a} + Q(\tilde{a}, \tilde{a}) + \tilde{L}_{\text{in}}\tilde{\gamma} + Q_{\text{in}}(\tilde{\gamma}, \tilde{\gamma}) + Q_{\text{ain}}(\tilde{a}, \tilde{\gamma}) \tag{16}$$

where

$$\tilde{L} = L + Q(\cdot, a_d) + Q(a_d, \cdot) + Q_{\text{ain}}(\cdot, \gamma_d)$$

$$\tilde{L}_{\text{in}} = L_{\text{in}} + Q_{\text{in}}(\gamma_d, \cdot) + Q_{\text{in}}(\cdot, \gamma_d) + Q_{\text{ain}}(a_d, \cdot)$$

For $\tilde{\gamma} = 0$, i.e., $\gamma = \gamma_d$, system (16) has an equilibrium at $\tilde{a} = 0$, which corresponds the desired state. We also eliminate $\gamma_{\text{inlet}}$ at this stage as it was a pseudoinput introduced for modeling purposes only. Under normal operation, we have $\gamma_{\text{inlet}} = 1$ (i.e., $\tilde{\gamma}_{\text{inlet}} = 0$) hence substitution into Eq. (16) yields a system of the same structure, with the corresponding dimensions of the matrices reduced by one. To keep the notation simple and avoid clutter, we will not introduce new names for these, but it will be understood from this point on that when referring to Eq. (16) we mean $\gamma = [\gamma_{\text{top}}\ \gamma_{\text{bottom}}]^T$ and $\tilde{\gamma} = [\tilde{\gamma}_{\text{top}}\ \tilde{\gamma}_{\text{bottom}}]^T$.

For the numerical simulation, one sees that the system (16) has an unstable equilibrium, as the eigenvalues of $\tilde{L}$ turn out to be $\{-1.4476 - 1.2619i, -1.4476 + 1.2619i, 0.3360, -0.1690\}$. The task is to stabilize the equilibrium with a domain of attraction large enough to include initial conditions of interest.

*Remark 4.1.* Note that for our system we have two controls, $\gamma_{\text{top}}$ and $\gamma_{\text{bottom}}$, which can only arbitrarily assign two points. The 2D profile $q_d$ to which we are attempting to drive the system through the controls contains an infinite number of points to assign, and the problem is therefore not feasible in general. The feasibility of the control objective is assured by the fact that the selected profile is within the reach of the augmented modes, i.e., $q_d \in \text{span}\{\varphi_i, \psi_i\}$, so that there exists a value of the control $\gamma_d$ that satisfies Eq. (15). Thus, there exists a value of the control that can maintain the system state at $a_d$, which corresponds to the desired 2D profile $q_d$.

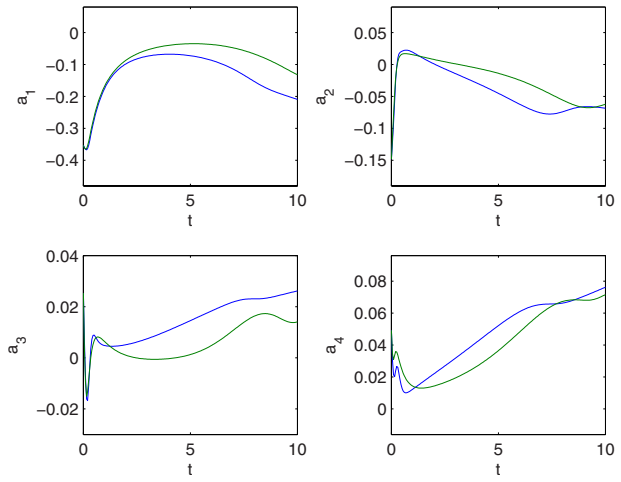


**Fig. 12 Response of Galerkin system (blue/dark) versus modal coefficients from direct projection (green/light)**

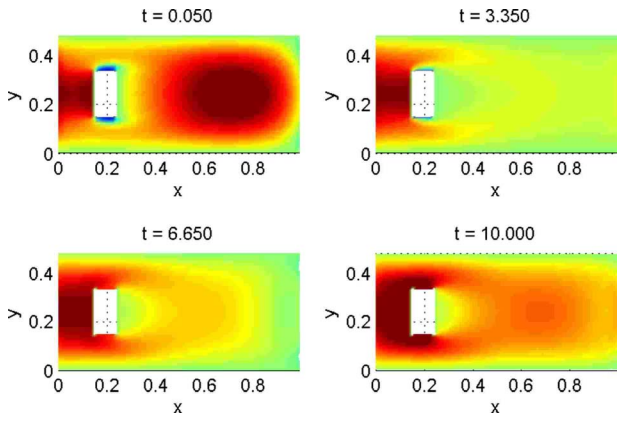


**Fig. 13 Reconstruction of the test flow in Fig. 11**

**4.1 Control Design Based on Averaging/Center Manifold Reduction.** The first approach to control design is based on phase-averaging and center manifold theory developed in Refs. [26,27], strongly inspired by the work of Noack et al. [10], Aamo and Krstic [30], Noack et al. [31], and Tadmor et al. [32] on suppression of cylinder wake instability. The proposed technique provides a means to reducing the Galerkin model Eq. (16) even further by looking at the behavior of an averaged system corresponding to Eq. (16), which evolves on a lower-dimensional submanifold of the state space and which exhibits useful symmetries in its structure. Phase-averaging is used here as a means of obtaining a Poincare' normal form of the closed-loop system under linear feedback [33,34]. The resulting normal form has the structure of a family of dynamical systems parametrized by the feedback gain. The structure of the parameter-dependent normal form allows further simplification, achieved by looking at the behavior of the dynamics on a locally attractive manifold called the center

manifold, which is described by only one coordinate. Here, we will provide a brief summary of the procedure for constructing the simplified reduced-order model, and refer the interested reader to Refs. [26,27].

As noted in Sec. 4, the eigenvalues of $\tilde{L}$ are of the form $\text{spec}(\tilde{L})=\{-\sigma+j\omega,-\sigma-j\omega,\lambda_1,-\lambda_2\}$ where $\sigma>0$, $\omega>0$, $\lambda_1,\lambda_2>0$. Using a nonsingular transformation, the system in Eq. (16) can be expressed in modal form as

$$\begin{aligned}\dot{\eta}&=F_1\eta+\varphi_1(\eta,\zeta)+G_1\gamma+\xi_1(\eta,\zeta,\gamma)\\ \dot{\zeta}&=F_2\zeta+\varphi_2(\eta,\zeta)+G_2\gamma+\xi_2(\eta,\zeta,\gamma)\end{aligned}\tag{17}$$

where

$$\eta=\begin{bmatrix}\eta_1\\ \eta_2\end{bmatrix},\quad \zeta=\begin{bmatrix}\zeta_1\\ \zeta_2\end{bmatrix},\quad F_1=\begin{bmatrix}-\sigma & -\omega\\ \omega & -\sigma\end{bmatrix},\quad F_2=\begin{bmatrix}\lambda_1 & 0\\ 0 & -\lambda_2\end{bmatrix}$$

$G_1, G_2\in\mathbb{R}^{2\times 2}$, and $\phi_1$, $\xi_1$, $\phi_2$, $\xi_2$ are continuously differentiable functions, which vanish at the origin together with their first derivatives. We will look for a control of the form $\gamma=K\,\text{col}(\eta,\zeta)$, where $\text{col}(\eta,\zeta)=[\eta^T\zeta^T]^T$. Substituting this into Eq. (17) yields

$$\begin{aligned}\dot{\eta}&=F_1\eta+\varphi_1(\eta,\zeta)+G_1K\,\text{col}(\eta,\zeta)+\xi_1(\eta,\zeta,K\,\text{col}(\eta,\zeta))\\ &:=f_\eta(\eta,\zeta,K)\\ \dot{\zeta}&=F_2\zeta+\varphi_2(\eta,\zeta)+G_2K\,\text{col}(\eta,\zeta)+\xi_2(\eta,\zeta,K\,\text{col}(\eta,\zeta))\\ &:=f_\zeta(\eta,\zeta,K)\end{aligned}\tag{18}$$

The approach that will be employed here involves the determination of a set of conditions on the gains $K$ so as to achieve the desired stabilization, and then set up a numerical optimization to find a set of gains that satisfy these criteria.

First, it will be required that the control does not alter the structure of the eigenvalue spectrum, i.e., the closed loop system will be assumed to have a spectrum of the form $\{-\sigma_m+j\omega_m,-\sigma_m-j\omega_m,-\lambda_{m1},-\lambda_{m2}\}$ where $\sigma_m,\omega_m,\lambda_{m1},\lambda_{m2}>0$. Respecting the original eigenvalue structure of the system, even in closed-loop, is important for preserving the domain of validity of reduced-order flow models, as discussed in depth in Refs. [26,27]. Transforming Eq. (18) into modal form gives

$$\begin{aligned}\dot{\eta}_m&=F_{m1}(K)\eta_m+\varphi_{m1}(\eta_m,\zeta_m,K)\\ \dot{\zeta}_m&=F_{m2}(K)\zeta_m+\varphi_{m2}(\eta_m,\zeta_m,K)\end{aligned}\tag{19}$$

where $\eta_m=\left[\begin{smallmatrix}\eta_{m1}\\ \eta_{m2}\end{smallmatrix}\right]$, $\zeta_m=\left[\begin{smallmatrix}\zeta_{m1}\\ \zeta_{m2}\end{smallmatrix}\right]$,

$$F_{m1}(K)=\begin{bmatrix}-\sigma_m & -\omega_m\\ \omega_m & -\sigma_m\end{bmatrix},\quad F_{m2}(K)=\begin{bmatrix}-\lambda_{m1} & 0\\ 0 & -\lambda_{m2}\end{bmatrix}$$

Following Eq. [10], we define a change in coordinates parametrized by a dummy variable $\vartheta\in[0,2\pi]$ described as $\eta^\vartheta=R(\vartheta)\eta_m$, where

$$R(\vartheta)=\begin{bmatrix}\cos\vartheta & \sin\vartheta\\ -\sin\vartheta & \cos\vartheta\end{bmatrix}$$

Using the above transformation and differentiating with respect to time, one obtains

$$\begin{aligned}\dot{\eta}^\vartheta&=R(\vartheta)f_\eta(R^T(\vartheta)\eta^\vartheta,\zeta_m,K)=:f_\eta^\vartheta(\vartheta,\eta^\vartheta,\zeta_m,K)\\ \dot{\zeta}_m&=f_\zeta(R^T(\vartheta)\eta^\vartheta,\zeta_m,K)=:f_\zeta^\vartheta(\vartheta,\eta^\vartheta,\zeta_m,K)\end{aligned}\tag{20}$$

Averaging over $\vartheta\in[0,2\pi]$, the following averaged system with states $\text{col}(\bar{\eta}^\vartheta,\bar{\zeta}^\vartheta)$ is obtained [10] by

$$\dot{\bar{\eta}}^\vartheta=\frac{1}{2\pi}\int_0^{2\pi}f_\eta^\vartheta(\vartheta,\bar{\eta}^\vartheta,\bar{\zeta}^\vartheta,K)d\vartheta=:f_{\eta,\text{avg}}^\vartheta(\bar{\eta}^\vartheta,\bar{\zeta}^\vartheta,K)$$

$$\dot{\bar{\zeta}}^\vartheta=\frac{1}{2\pi}\int_0^{2\pi}f_\zeta^\vartheta(\vartheta,\bar{\eta}^\vartheta,\bar{\zeta}^\vartheta,K)d\vartheta=:f_{\zeta,\text{avg}}^\vartheta(\bar{\eta}^\vartheta,\bar{\zeta}^\vartheta,K).$$

From this point on, for ease of notation, we will drop the bars and superscripts $\vartheta$ from the variables $\eta$, $\zeta$, $\sigma$, $\omega$, and $\lambda$. More precisely, from now on $\bar{\eta}^\vartheta$ will be denoted by $\eta$, $\bar{\zeta}^\vartheta$ by $\zeta$, $f_{\eta,\text{avg}}^\vartheta$ by $f_{\eta,\text{avg}}$, and $f_{\zeta,\text{avg}}^\vartheta$ by $f_{\zeta,\text{avg}}$. The averaged system is then written as

$$\begin{aligned}\dot{\eta}&=f_{\eta,\text{avg}}(\eta,\zeta,K)\\ \dot{\zeta}&=f_{\zeta,\text{avg}}(\eta,\zeta,K)\end{aligned}\tag{21}$$

Converting the averaged system above into polar coordinates, i.e., $\rho=\sqrt{\eta_1^2+\eta_2^2}$ and $\theta=\arctan(\eta_2/\eta_1)$, and viewing the constant $\sigma_m$ as a state with trivial dynamics, one can write

$$\begin{aligned}\begin{bmatrix}\dot{\sigma}_m\\ \dot{\rho}\end{bmatrix}&=\begin{bmatrix}0 & 0\\ 0 & 0\end{bmatrix}\begin{bmatrix}\sigma_m\\ \rho\end{bmatrix}+\begin{bmatrix}0\\ \varphi_{12}(\sigma_m,\rho,\zeta,K)\end{bmatrix}\\ \begin{bmatrix}\dot{\zeta}_1\\ \dot{\zeta}_2\end{bmatrix}&=F_{m2}(K)\begin{bmatrix}\zeta_1\\ \zeta_2\end{bmatrix}+\begin{bmatrix}\varphi_{21}(\sigma_m,\rho,\zeta,K)\\ \varphi_{22}(\sigma_m,\rho,\zeta,K)\end{bmatrix}\end{aligned}\tag{22}$$

where $\phi_{12}$ and $\phi_2=[\phi_{21}\ \phi_{22}]^T$ collect the nonlinear terms in Eq. (22) and $\phi_{12}(0,0,0,K)=0$ and $\phi_2(0,0,0,K)=0$ for any $K$.

*Remark 4.2*. The dynamics of $\rho$ in Eq. (22) is actually of the form $\dot{\rho}=-\sigma_m\rho+\ldots$. Looking at $\sigma_m$ as a state renders the term $-\sigma_m\rho$ a nonlinear function of the state variables, therefore it is collected in $\phi_{12}$. This makes it possible to view $\sigma_m$ and $\rho$ as center states and thus apply the center manifold theory [35].

*Remark 4.3*. Note that none of the state dynamics in Eq. (22) depend on $\theta$. Therefore the dynamics of the state variable $\theta$ are immaterial as far as the stabilization of system (22)is concerned.

Recall that the gains $K$ are selected such that $F_{m2}$ is Hurwitz, so this partitions the system in Eq. (22) into center states $\sigma_m$ and $\rho$, and stable states $\zeta_1$ and $\zeta_2$. This allows one to perform an analysis of the system (22) on a center manifold, which is guaranteed to exist per center manifold theory [35]. The center manifold is an invariant manifold of the form $\zeta=\bar{\zeta}(\sigma_m,\rho)$, where $\bar{\zeta}=[\bar{\zeta}_1\bar{\zeta}_2]^T$, satisfying

$$\frac{\partial\bar{\zeta}_i}{\partial\rho}\varphi_{12}(\sigma_m,\rho,\bar{\zeta}(\sigma_m,\rho),K)=-\lambda_{mi}\bar{\zeta}_i(\sigma_m,\rho)+\varphi_{2i}(\sigma_m,\rho,\bar{\zeta}_i(\sigma_m,\rho),K)\tag{23}$$

for $i=1,2$, to which the dynamics of the system (22) will be locally attracted. The differential equations in Eq. (23) cannot be solved directly, so one needs to look for an approximation of the form

$$\bar{\zeta}_i(\rho,\sigma_m)=c_{i,1}(K)\sigma_m^2+c_{i,2}(K)\sigma_m\rho+c_{i,3}(K)\rho^2+\mathcal{O}(\rho^3)\tag{24}$$

for $i=1,2$. One then substitutes Eq. (24) into Eq. (23) and solves for the coefficients. Then substituting Eq. (24) into Eq. (22) gives the system dynamics on the approximate center manifold, which is of the form

$$\dot{\rho}=(d_1(K)+d_2(K)\rho+d_3(K)\rho^2)\rho\tag{25}$$

where parameters $d_i$ depend on parameters $c_{i,j}$ in Eq. (24).

*Remark 4.4*. It will be useful at this point to restate how the final reduced-order system in Eq. (25) is theoretically related to the full-order Galerkin system in modal form in Eq. (17). The first step of the reduction process is averaging, as a result of which Eq. (17) is reduced to the averaged system (21). The process is based on the averaging theory, which guarantees the existence of a neighborhood around the origin in which the trajectories of the original system (17) are arbitrarily close to that of the averaged system (21). The second step of the reduction process is center manifold reduction, as a result of which the averaged system (21)

is reduced to the system on the center manifold (25). The process is based on the center manifold theory, which guarantees the existence and invariance of such a manifold, and that the trajectories of the system (21) will be locally attracted to the trajectories of the corresponding system on the center manifold, namely, system (25). To summarize, the trajectories of the Galerkin system (17) are locally close to that of the averaged system (21), and the trajectories of the averaged system (21) are locally close to that of the system on the center manifold (25). Joining these two results, one can conclude that there exists a neighborhood in which the stability properties of the Galerkin system (17) are preserved in this neighborhood for the final reduced-order system on the center manifold in Eq. (25). Therefore, provided that one is not too aggressive with the control design and stays in this neighborhood, designing a control based on system (25) and then applying it to the full-order Galerkin system in Eq. (17) is a theoretically valid approach. Detailed mathematical derivations as to how these theoretical links between the models are established precisely could not be given in this paper due to space limitations and to avoid repetition with our previous works; the interested reader is referred to Refs. [26,27].

Explicit expressions for the parameters in the above derivations are complicated and difficult to analyze analytically, so a numerical search problem over the range $K_{ij} \in [-150, 150]$ for $i=1,2j=1,\ldots,4$ is implemented to select proper values for $K$ to satisfy the following criteria.

1. The original eigenvalue structure of the system is respected in closed-loop, i.e., the gains $K$ must be chosen such that the closed-loop spectrum is of the form $\{-\sigma_m + j\omega_m, -\sigma_m - j\omega_m, -\lambda_{m1}, -\lambda_{m2}\}$ where $\sigma_m, \omega_m, \lambda_{m1}, \lambda_{m2} > 0$.
2. The center manifold needs to be attractive for $\zeta \in Z$ and $\rho \in D$ for some given domains $Z$ and $D$ that include the initial conditions of interest. More precisely, we define the off-manifold distance as $\tilde{\zeta} := \zeta - \bar{\zeta}(\sigma_m, \rho)$. Differentiating yields the off-manifold dynamics which has the form

$$\dot{\tilde{\zeta}} = F_{m2}(K)\tilde{\zeta} + \varphi_3(\sigma_m, \rho, \tilde{\zeta}, K) \tag{26}$$

for which $\tilde{\zeta}=0$ is an equilibrium as the center manifold is invariant, and $\phi_3$ collects nonlinear terms. We define a candidate Lyapunov function as

$$V := \tilde{\zeta}^T P \tilde{\zeta} \tag{27}$$

where $P=P^T>0$ is the solution to the Lyapunov equation $PF_{m2}^T + F_{m2}P = -I$. This choice for $P$ is the one that maximizes the estimate for the domain of attraction [36]. Differentiating Eq. (27) yields the time derivative $\dot{V}$ of the form

$$\dot{V} = 2\tilde{\zeta}^T P F_{m2}(K)\tilde{\zeta} + 2\tilde{\zeta}^T P \varphi_3(\sigma_m, \rho, \tilde{\zeta}, K) \tag{28}$$

To achieve convergence of trajectories to the manifold, one then needs to have $\dot{V}<0$ for $\rho \in D$ and $\tilde{\zeta} \in Z$, where $Z$ needs to be large enough to include a level set of $V$ containing the value of $\tilde{\zeta}(0)$ corresponding to the initial condition of interest.
3. The center manifold dynamics needs to be such that $\rho$ converges to zero on the manifold, for $\rho \in D$. Consider the on-manifold dynamics in Eq. (25). We define a candidate Lyapunov function as

$$V := \rho^2 \tag{29}$$

and differentiate to get

$$\dot{V} = 2\rho^2(d_1(K) + d_2(K)\rho + d_3(K)\rho^2) \tag{30}$$

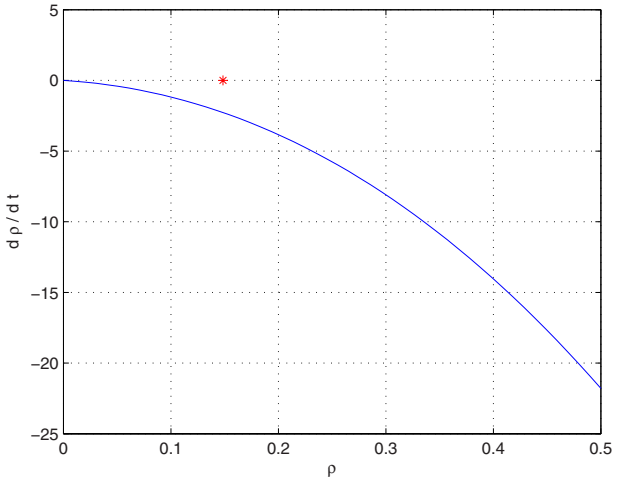


**Fig. 14 $\dot{\rho}$ versus $\rho$ for the on-manifold dynamics. The star denotes the value of $\rho(0)$ corresponding to the given initial condition.**

To achieve convergence of $\rho$ to 0, once the trajectories of the system are close to the center manifold, one needs to have the condition $\dot{V}<0$ satisfied for all $\rho \in D$, where the set $D$ must be large enough to contain the value of $\rho(0)$ corresponding to the initial condition of interest. Since in Eq. (30) the term $2\rho^2$ is non-negative, the condition $\dot{V}<0$ is equivalent to having $(d_1(K) + d_2(K)\rho + d_3(K)\rho^2) < 0$ for all $\rho \in D$.

*Remark 4.5.* The first item above, i.e., the problem of maintaining of the eigenvalue structure, can actually be considered at the level of the linearization of Eq. (17). The reason why we have grouped it together with all the other criteria is that it is much more efficient to implement a one-step numerical search for $K$ to satisfy all the criteria at once. A two step-search procedure where we first determine a value for $K$ that keeps the eigenvalue structure, and then check if it satisfies the other two criteria, and keep iterating back and forth would be much more time consuming and computationally intensive.

In the numerical implementation of the algorithm, initialization of the search from a randomly selected value $K_0$ such that $K_{0ij} \in [-150, 150]$ for $i=1,2j=1,\ldots,4$, yielded a successful termination at

$$K = \begin{bmatrix} 0.0297 & 37.0349 & -39.4230 & 37.0349 \\ 0.0297 & 37.0349 & -39.4230 & 37.0349 \end{bmatrix}$$

which satisfies all the required criteria. Figure 14 shows a plot of the on-manifold dynamics $\dot{\rho}$ versus $\rho$ for the gains above. The value of $\rho$ corresponding to our initial point of interest is also marked on the plot. It can be seen that the gains render $\dot{\rho}<0$ for $\rho$ in the domain $D=[0, 0.5]$, which includes the value of $\rho$ of interest. Figure 15 shows the Lyapunov function (27) for the off-manifold behavior, where $\tilde{\zeta}$ is in the domain $Z=[-0.4, 0.4] \times [-0.4, 0.4]$, which includes the value of $\tilde{\zeta}$ corresponding to the initial condition and some level sets containing it. Figure 16 shows the derivative of $V$ for some values of $\rho$ in $D$. It can be seen that $\dot{V}$ is negative for $\tilde{\zeta} \in Z$ and $\rho \in D$. Figure 17 shows the application of the controller resulting from these gains to the nonlinear Galerkin system in Eq. (16). It can be seen that the desired stabilization is achieved for this controller. The control is then tested in the full-order Burgers' simulation, which is shown Fig. 18. The control input signals applied are shown in Fig. 19. Also, Fig. 20 shows a comparison of the desired state, final state, and the absolute error between the two. It can be seen that the averaging/center

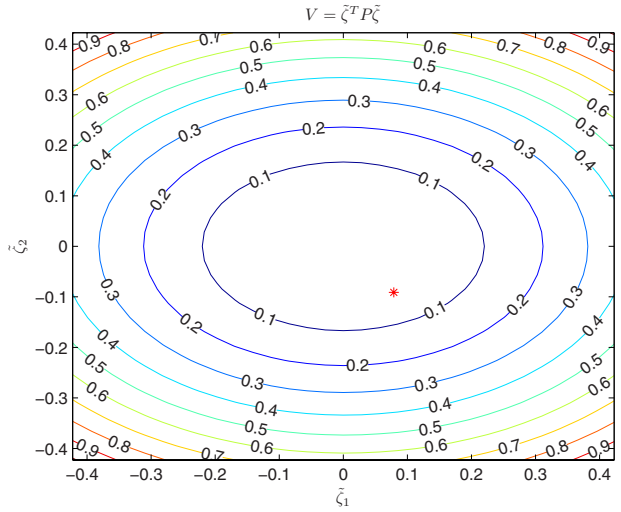


**Fig. 15 Lyapunov function *V* for the off-manifold dynamics. The star denotes the value of $\tilde{\zeta}(0)$ corresponding to the given initial condition.**

manifold based design achieves the desired regulation with very small error for the most part of the domain.

**4.2 (LQR) Control Design Based on Linearization.** In this section, a linearization-based LQR controller will be developed for comparison purposes. A similar linearization/LQR design on the model problem was utilized in Ref. [21] on weak formulation based reduced-order models. While LQR design based on linearization is not a new approach, our purpose in presenting it is to provide a means to evaluate the novel averaging/CM method approach just presented. Recall that averaging/CM method achieves control design through a nonlinear analysis, utilizing averaging theory and center manifold theory. As indicated in Remark 4.4, both of these are local theories and therefore the results obtained are local in nature as well. One may therefore question if it is worth going through the trouble of carrying out the relatively complicated steps of the averaging/CM method, while another local technique, namely, the linearization/LQR method, provides an easier and a more standard implementation. To answer this question, we implement the linearization/LQR method to obtain

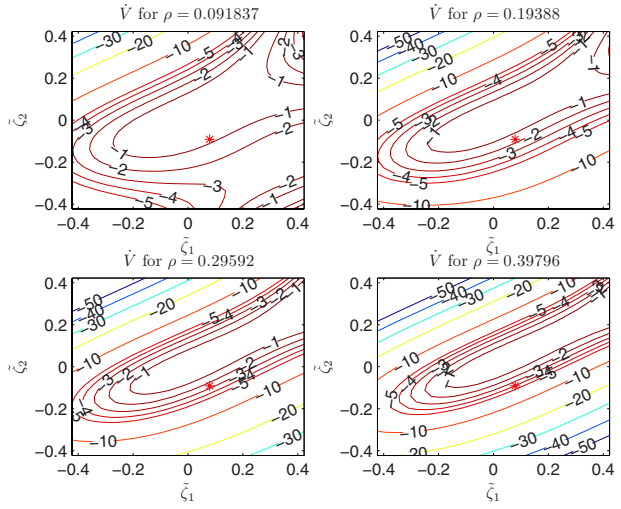


**Fig. 16 Derivative of Lyapunov function *V* for the off-manifold dynamics for different values of $\rho$. The star denotes the value of $\tilde{\zeta}(0)$ corresponding to the given initial condition.**

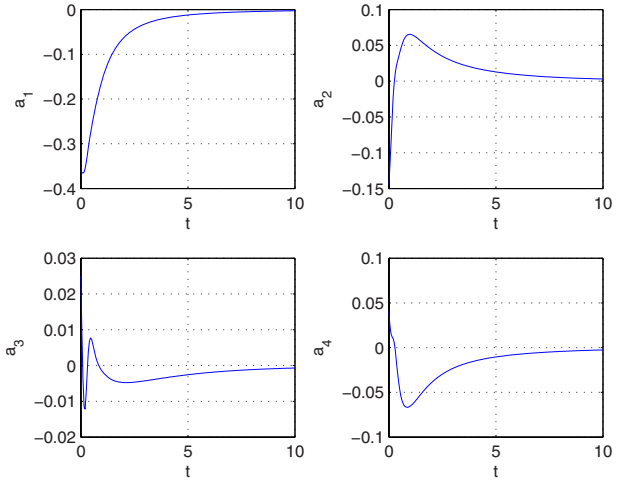


**Fig. 17 Modal coefficients *a*(*t*) of the closed-loop system with control derived from averaging/center manifold theory**

numerical simulations on Galerkin models and CFD simulations on full-order Burgers' models and compare these results with those obtained earlier for the averaging/CM method.

For the linearization/LQR design, we start with the linearization of the system (16), which is

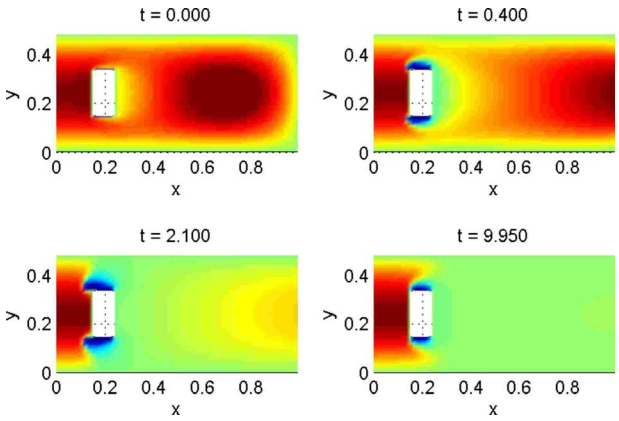


**Fig. 18 Averaging/center manifold-based control applied to full order Burgers' CFD**

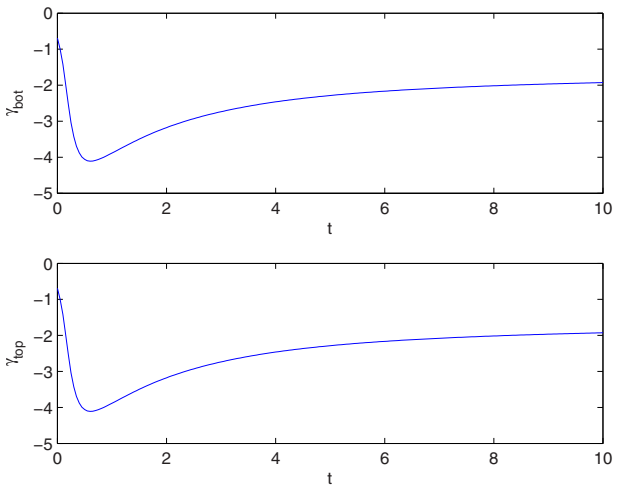


**Fig. 19 Control signals for averaging/center manifold-based control**

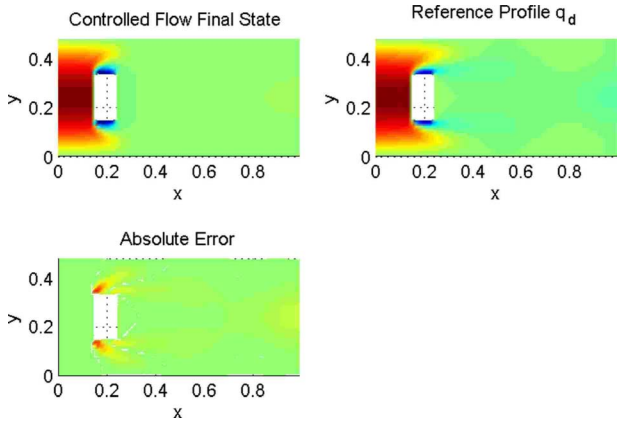


**Fig. 20 Final state, reference profile, and absolute error for averaging/center manifold-based control**

$$\dot{\tilde{a}} = \tilde{L}\tilde{a} + \tilde{L}_{\text{in}}\tilde{\gamma}$$

Classical LQR control attempts to design a control law of the form $\tilde{\gamma}=-K\tilde{a}$, where $K$ is selected to minimize the objective function

$$J(\tilde{\gamma}) = \int_0^\infty (a^T Q a + \tilde{\gamma}^T R \tilde{\gamma}) dt \tag{31}$$

Despite numerous trials with many different values for the weighing parameters $Q$ and $R$, it was not possible to obtain a controller that achieves stabilization starting from the desired initial condition $a_0$, when the control was applied to the nonlinear Galerkin system in Eq. (16). For this reason, a modification of the standard LQR approach was used, as proposed in Refs. [21,37]. This approach tries to minimize a modified objective function of the form

$$J(\tilde{\gamma}) = \int_0^\infty (a^T Q a + \tilde{\gamma}^T R \tilde{\gamma}) e^{2\alpha t} dt \tag{32}$$

where $\alpha > 0$ is an additional parameter to be selected. After a number of trials with different values for $\alpha$, $Q$, and $R$, the best results were obtained for $\alpha=0.1$, $Q=2500I_4$, and $R=I_2$. The resulting controller is of the form $\tilde{\gamma}=-K\tilde{a}$ with

$$K = \begin{bmatrix} -27.9149 & 117.1223 & 50.2110 & -52.4688 \\ -27.9159 & 117.1197 & 50.2104 & -52.4673 \end{bmatrix}$$

Figure 21 shows the result of the implementation of this control law on the nonlinear Galerkin system (16). It can be seen that control achieves the desired stabilization, but the response is not as smooth and nice compared to the the response obtained using the averaging/center manifold controller in Fig. 17. The control is also implemented in the full order Burgers' CFD simulation, which is shown Fig. 22. The control input signals applied are shown in Fig. 23. Figure 24 shows a comparison of the desired state, final state, and the absolute error between the two. It can be seen that the control achieves the regulation with small error for the most part of the domain. However, the control effort is higher compared to that of the averaging/center manifold controller (see Fig. 19), and for the parts of the domain where the error is visible, its value is notably higher than the averaging/center manifold case (see Fig. 20).

*Remark 4.6*. Note that for both averaging/CM and linearization/LQR approaches, the control law has a linear structure. One may, therefore, wonder what would happen if we used a control law with nonlinear terms. Such an approach was actually considered in Refs. [26,27], where the problem of reducing oscillations induced by air flow over a shallow cavity were attacked using averaging/CM methods for control laws that are purely nonlinear,

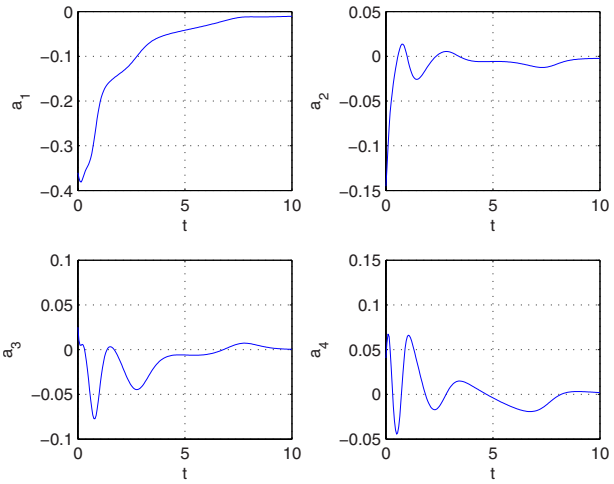


**Fig. 21 Modal coefficients $a(t)$ of the closed-loop system with LQR control**

i.e., have no linear part at all. In these problems, total suppression of oscillations is not physically realistic but only a reduction in amplitude is possible. One, therefore, always operates far away from the equilibrium point, hence the use of purely nonlinear control laws. For the particular problem at hand, it may certainly be of benefit for the control law to have a nonlinear part, which is something that we plan on investigating as part of our future

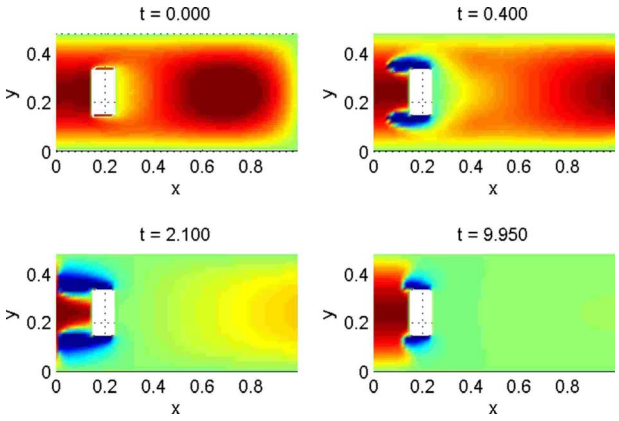


**Fig. 22 LQR control applied to full order Burgers' CFD**

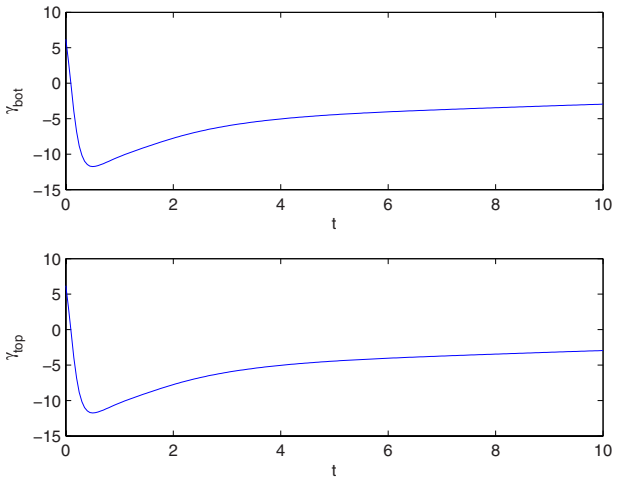


**Fig. 23 Control signals for LQR control**

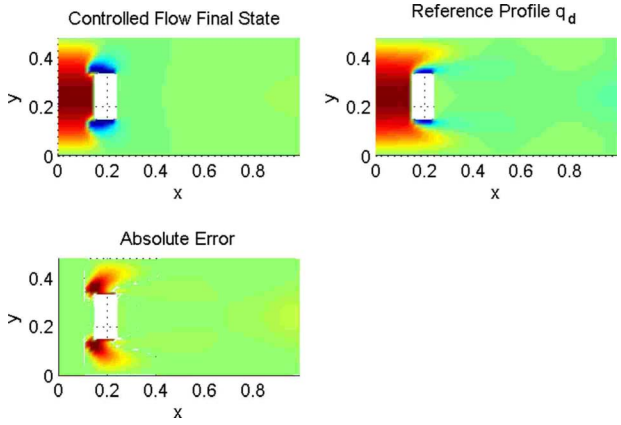


**Fig. 24 Final state, reference profile, and absolute error for LQR control**

works. There is, however, one advantage of using a linear control law, which is to provide a better comparison with the standard linearization based LQR approach. When the control laws are of the same kind, i.e., $\gamma = K\tilde{a}$, the better performance achieved by the first controller can directly be attributed to the averaging/CM techniques, and not to the additional degree of freedom or the presence of alternative terms. Although both the averaging/CM and linearization based methods are local and design a controller with the same structure, the analysis through averaging/CM is somewhat "less local" as it attempts to incorporate the nonlinearities into the reduced model, whereas the linearization method simply ignores them.

## 5 Concluding Remarks

In this paper, we studied a sample boundary control problem, governed by the two-dimensional Burgers' equation, describing convective flow over an obstacle. A reduced-order model was built based on a POD expansion consisting of baseline modes and actuation modes, where the former were built using unactuated snapshots and the latter were built in an energy optimal fashion using innovation vectors, which represent the flow not captured by the baseline space. This was followed by a controller design with the control objective of driving the system state to a desired 2D profile. The controller design was based on an analysis using averaging theory and center manifold theory to further simplify the system and reveal more structure. From this analysis, certain conditions for the controller gains to satisfy were derived, and a numerical search problem was set up and numerically solved. For comparison, a standard LQR design based on the linearization of the reduced-order model was implemented and tested. It was seen through full order simulations that while both controllers achieve the desired objective, the averaging/center manifold based controller design results in a smoother response with less control effort and smaller tracking error over the problem domain.

We believe that the importance and contribution of this work is that it provides a complete reduced-order modeling and subsequent nonlinear control design approach for a general class of distributed parameter model problem with control actuation at the boundary of the spatial domain. The development of order reduction methods and nonlinear control techniques for boundary control configurations is an open problem. This work proposes a way to address some of the issues in that regard, at least as far as reduced-order model-based control is concerned. The approaches to reduced-order modeling and control design proposed in this work presents advantages over their classical counterparts. For the $\mathcal{L}_2$ optimization method used in modeling, the advantage is that the input is rendered as an explicit term in the reduced-order model in an optimal sense, that is, by minimizing the energy neglected by the augmented POD expansion. This is an improvement over standard POD/GP reduced-order modeling methods, as in those cases the input remains embedded into the systems coefficients. It also constitutes an improvement over other input separation methods, such as the weak formulation method that was used in earlier works for this problem. Boundary input separation methods based on a weak formulation of the Galerkin projection rely on finely partitioned data near the control input in order to accurately approximate boundary derivatives and make boundary control inputs explicit. These approaches may not lend themselves easily to order reduction using experimental data as grid resolution near the boundary is difficult to refine in experiment. The $\mathcal{L}_2$ optimization method captures the boundary control input indirectly and lends itself easily to both computational and experimental order reduction approaches. As far as the control strategy is concerned, the averaging/center manifold-based design offers the advantage that the system is reduced to a single state system on a center manifold, which is much easier to analyze and control than the original Galerkin model. This simplification still captures more characteristics of the original system as compared to simple linearization. This was seen from the comparison of the control designed by this method and that designed by linearization followed by LQR, where it was observed that the overall error was less for the averaging/center manifold case while requiring less control power. It is hoped that the presentation of the entire process from reduced modeling suitable for boundary actuation to subsequent nonlinear control design for the distributed parameter model problem discussed in this paper may provide better insight to leverage these methods for application in other flow control problems as well. As an example, future research directions include the implementation of these methods to reduce or eliminate flow separation over an airfoil with a simply hinged flap. These methods are also currently being utilized to reduce optical beam distortion due to turbulent fluid flow for an aero-optic application.

## Acknowledgment

This work was supported by AFOSR and AFRL through the Collaborative Center of Control Science at OSU (Contract No. F33615-01-2-3154).

## Appendix: Proof of Theorem 3.1

The proof of Theorem 3.1 was given in detail in Ref. [23] and is repeated here for convenience of the reader.

Theorem. *Let* $J(\psi) := E[\|\tilde{q}_k - \gamma_k \psi\|^2]$. *Then*,

1. *The minimum value of the function J is achieved at* $\psi^* = E[\gamma_k \tilde{q}_k]/E[(\gamma_k)^2]$.
2. $\psi^* \in \mathbb{H}$.
3. $\psi^* \perp \varphi_i$ *for* $i = 1, \ldots, N$.

*Proof*

1. Note that

$$J(\psi) = E[\|\tilde{q}_k\|^2 - 2\gamma_k \langle \tilde{q}_k, \psi \rangle + (\gamma_k)^2 \|\psi\|^2]$$

Since $J$ is quadratic in $\psi$ with a positive leading coefficient, it has a unique minimum. Computing the first variation of $J$ with respect to $\xi \in \mathbb{H}$ yields

$$\frac{d}{d\delta}\bigg|_{\delta=0} J(\psi + \delta\xi) = \frac{d}{d\delta}\bigg|_{\delta=0} E[\|\tilde{q}_k\|^2 - 2\gamma_k \langle \tilde{q}_k, \psi + \delta\xi \rangle + \gamma_k^2 \|\psi + \delta\xi\|^2] = \langle E[-2\gamma_k \tilde{q}_k + 2\gamma_k^2 \psi], \xi \rangle$$

For $\psi$ to be an extremum of $J$, its first variation must vanish $\forall \xi \in \mathbb{H}$. Therefore, $E[-2\gamma_k \tilde{q}_k + 2\gamma_k^2 \psi^*] = 0$ and thus, by linearity of $E$, $\psi^* = E[\gamma_k \tilde{q}_k]/E[\gamma_k^2]$.

2. The fact that $\psi^* \in \mathbb{H}$ follows from the fact that $E$ is linear, $\gamma_k \tilde{u}_k \in \mathbb{H}$, and $E[(\gamma_k)^2] \in \mathbb{R}$.

3. To show that $\psi^* \perp \varphi_i$ for $i=1,\ldots,N$, first note that $\tilde{q}_k \perp S$ for all $k=1,\ldots,N$. For any $i$ and $k$,

$$\langle \tilde{q}_k, \phi_i \rangle = \langle q - P_S q, \phi_i \rangle = \left\langle q - \sum_{j=1}^{n} \langle q, \phi_j \rangle \phi_j, \phi_i \right\rangle = \langle q, \phi_i \rangle - \sum_{j=1}^{n} \langle q, \phi_j \rangle \langle \phi_j, \phi_i \rangle = 0$$

Then, for any $i$, using the above result, the linearity of $E$ and the linearity of the inner product, one obtains

$$\langle \psi^*, \phi_i \rangle = \left\langle \frac{E[\gamma_k \tilde{q}_k]}{E[\gamma_k^2]}, \phi_i \right\rangle = \frac{E[\gamma_k \langle \tilde{q}_k, \phi_i \rangle]}{E[\gamma_k^2]} = 0$$

Therefore, it follows that $\psi^* \perp S$.

□

## References


[1] Smaoui, N., 2005, "Boundary and Distributed Control of the Viscous Burgers Equation," J. Comput. Appl. Math., **182**(1), pp. 91–104.

[2] Hinze, M., and Kunisch, K., 2004, "Second Order Methods for Boundary Control of the Instationary Navier–Stokes System," ZAMM, **84**(3), pp. 171–87.

[3] Kobayashi, T., and Oya, M., 2003, "Nonlinear Boundary Control of Coupled Burgers' Equations," Contr. Cybernet., **32**(2), pp. 245–58.

[4] Park, H. M., and Lee, M. W., 2000, "Boundary Control of the Navier–Stokes Equation by Empirical Reduction of Modes," Comput. Methods Appl. Mech. Eng., **188**(1–3), pp. 165–86.

[5] Krstic, M., 1999, "On Global Stabilization of Burgers' Equation by Boundary Control," Syst. Control Lett., **37**(3), pp. 123–41.

[6] Aamo, O. M., Krstic, M., and Bewley, T. R., 2003, "Control of Mixing by Boundary Feedback in 2D Channel Flow," Automatica, **39**(10), pp. 1597–1606.

[7] Anderson, J. D., 1995, *Computational Fluid Dynamics: The Basics With Applications*, McGraw Hill, New York.

[8] Kook, H., Mongeau, L., and Franchek, M. A., 2002, "Active Control of Pressure Fluctuations Due to Flow Over Helmholtz Resonators," J. Sound Vib., **255**(1), pp. 61–76.

[9] Rowley, C. W., Colonius, T., and Murray, R. M., 2004, "Model Reduction for Compressible Flows Using POD and Galerkin Projection," Physica D, **189**(1–2), pp. 115–29.

[10] Noack, B. R., Afanasiev, K., Morzynski, M., Tadmor, G., and Thiele, F., 2003, "A Hierarchy of Low-Dimensional Models for the Transient and Post-Transient Cylinder Wake," J. Fluid Mech., **497**, pp. 335–63.

[11] Rempfer, D., 2000, "On Low-Dimensional Galerkin Models for Fluid Flow," Theor. Comput. Fluid Dyn., **14**(2), pp. 75–88.

[12] Holmes, P., Lumley, J. L., and Berkooz, G., 1996, *Turbulence, Coherent Structures, Dynamical System, and Symmetry*, Cambridge University Press, Cambridge.

[13] Noack, B. R., and Eckelmann, H., 1994, "A Global Stability Analysis of the Steady and Periodic Cylinder Wake," J. Fluid Mech., **270**, pp. 297–330.

[14] Noack, B. R., Papas, P., and Monkewitz, P. A., 2005, "The Need for a Pressure-Term Representation in Empirical Galerkin Models of Incompressible Shear Flows," J. Fluid Mech., **523**, pp. 339–65.

[15] Rowley, C. W., and Marsden, J. E., 2000, "Reconstruction Equations and the Karhunen–Loeve Expansion for Systems With Symmetry," Physica D, **142**(1–2), pp. 1–19.

[16] Fitzpatrick, K., Feng, Y., Lind, R., Kurdila, A. J., and Mikolaitis, D. W., 2005, "Flow Control in a Driven Cavity Incorporating Excitation Phase Differential," J. Guid. Control Dyn., **28**(1), pp. 63–70.

[17] Samimy, M., Debiasi, M., Caraballo, E., Serrani, A., Yuan, X., Little, J., and Myatt, J. H., 2007, "Feedback Control of Subsonic Cavity Flows Using Reduced-Order Models," J. Fluid Mech., **579**, pp. 315–346.

[18] Singh, S. N., Myatt, J. H., Addington, G. A., Banda, S., and Hall, J. K., 2001, "Optimal Feedback Control of Vortex Shedding Using Proper Orthogonal Decomposition Models," ASME Trans. J. Fluids Eng., **123**(3), pp. 612–618.

[19] Hogberg, M., Bewley, T. R., and Henningson, D. S., 2001, "Linear Feedback Control and Estimation of Transition in Plane Channel Flow, J. Fluid Mech., **481**, pp. 149–175.

[20] Camphouse, R. C., 2005, "Boundary Feedback Control Using Proper Orthogonal Decomposition Models," J. Guid. Control Dyn., **28**, pp. 931–938.

[21] Camphouse, R., Myatt, J., Schmit, R., Glauser, M., Ausseur, J., Andino, M., and Wallace, R., 2008, "A Snapshot Decomposition Method for Reduced Order Modeling and Boundary Feedback Control," AIAA Paper No. 2008-4195.

[22] Efe, M. O., and Ozbay, H., 2004, "Low Dimensional Modelling and Dirichlet Boundary Controller Design for Burgers Equation," Int. J. Control, **77**(10), pp. 895–906.

[23] Kasnakoglu, C., Serrani, A., and Efe, M. O., 2008, "Control Input Separation by Actuation Mode Expansion for Flow Control Problems," Int. J. Control, **81**(9), pp. 1475–1492.

[24] Hunt, J. C. R., Abell, C. J., Peterka, J. A., and Woo, H., 1978, "Kinematical Studies of the Flows Around Free or Surface-Mounted Obstacles; Applying Topology to Flow Visualization," Journal of Fluid Mechanics Digital Archive, **86**, pp. 179–200.

[25] Orellano, A., and Wengle, H., 2000, "Numerical Simulation (DNS and LES) of Manipulated Turbulent Boundary Layer Flow Over a Surface-Mounted Fence," Eur. J. Mech. B/Fluids, **19**, pp. 765–788.

[26] Kasnakoglu, C., and Serrani, A., 2007, "Oscillation Supression in Galerkin Systems Using Center-Manifold and Averaging Techniques," Eur. J. Control, **5**(13), pp. 529–542.

[27] Kasnakoglu, C., and Serrani, A., 2007, "Analysis and Nonlinear Control of Galerkin Models Using Averaging and Center Manifold Theory," *American Control Conference*, New York, pp. 3035–3040.

[28] Camphouse, R. C., and Myatt, J. H., 2004, "Feedback Control for a Two-Dimensional Burgers Equation System Model," *Second AIAA Flow Control Conference*, Portland, OR.

[29] Batchelor, G. K., 2000, *An Introduction to Fluid Dynamics*, Cambridge University Press, Cambridge, United Kingdom.

[30] Aamo, O. M., and Krstic, M., 2004, "Feedback Control of Particle Dispersion in Bluff Body Wakes," Int. J. Control, **77**(11), pp. 1001–1018.

[31] Noack, B. R., Tadmor, G., and Morzynski, M., 2004, "Low-Dimensional Models for Feedback Flow Control. Part I: Empirical Galerkin Models," *Proceedings of the Second AIAA Flow Control Conference*, Portland, OR, AIAA Paper No. 2004-2408.

[32] Tadmor, G., Noack, B. R., Morzynski, M., and Siegel, S., 2004, "Low-Dimensional Models for Feedback Flow Control. Part II: Controller Design And Dynamic Estimation," *Proceedings of the Second AIAA Flow Control Conference*, Portland, OR, AIAA Paper No. 2004-2409.

[33] Marsden, J. E., and McCracken, M., 1976, *The Hopf Bifurcation and Its Applications*, Springer-Verlag, New York, NY.

[34] Chow, S. N., and Mallet-Paret, J., 1977, "Integral Averaging and Bifurcation," J. Differ. Equations, **26**(1), pp. 112–159.

[35] Wiggins, S., 2003, *Introduction to Applied Nonlinear Dynamical Systems and Chaos*, Springer-Verlag, New York, NY, 2nd edition.

[36] Vidyasagar, M., 2002, *Nonlinear Systems Analysis*, 2nd ed., Society for Industrial and Applied Mathematics, Philadelphia, PA.

[37] Burns, J., and Kang, S., 1991, "A Control Problem for Burgers Equation With Bounded Input/Output," Nonlinear Dyn., **2**, pp. 235–262.